

Weighted lens depth: Some applications to supervised classification

Alejandro Cholaquidis¹, Ricardo Fraiman¹
Fabrice Gamboa² and Leonardo Moreno³

¹ Centro de Matemáticas, Facultad de Ciencias, Universidad de la República, Uruguay.

² Institut de Mathématiques de Toulouse, France.

³ Instituto de Estadística, Departamento de Métodos Cuantitativos, FCEA, Universidad de la República, Uruguay.

Abstract

Starting with Tukey’s pioneering work in the 1970’s, the notion of depth in statistics has been widely extended especially in the last decade. These extensions include high dimensional data, functional data, and manifold-valued data. In particular, in the learning paradigm, the depth–depth method has become a useful technique. In this paper we extend the notion of lens depth to the case of data in metric spaces, and prove its main properties, with particular emphasis on the case of Riemannian manifolds, where we extend the concept of lens depth in such a way that it takes into account non-convex structures on the data distribution. Next we illustrate our results with some simulation results and also in some interesting real datasets, including pattern recognition in phylogenetic trees using the depth–depth approach.

1 Introduction

The notion of depth was first introduced in statistics by Tukey in the 70’s, see Tukey (1975), for multivariate data. It is defined on \mathbb{R}^d by the Tukey depth function $\text{TD}(x, P) : \mathbb{R}^d \rightarrow [0, \infty)$ given by $\text{TD}(x, P) := \inf\{P(H) : H \text{ a closed halfspace, } x \in H\}$, for a probability measure P on \mathbb{R}^d . Roughly speaking, given P , $\text{TD}(x, P)$ measures how deep x is with respect to P . Following that seminal paper, several notions of depth were proposed and developed. Two other important and well established notions of depth are the simplicial depth and the spatial depth. The simplicial depth, introduced by Liu, see Liu (1990, 1992); Liu and Singh (1992), is defined by $\text{SD}(x, P_X) := \mathbb{P}(x \in S[X_1, \dots, X_{d+1}])$, where X_1, \dots, X_{d+1} is an iid sample of \mathbb{R}^d with common distribution P_X , and $S[X_1, \dots, X_{d+1}]$ is the d -dimensional simplex with vertices X_1, \dots, X_{d+1} , that is, the set of all possible convex combinations of the sample points. Spatial depth, introduced by Serfling, see Serfling (2002); Vardi and Zhang (2000), is defined by $\text{SpD}(x, P) = 1 - \mathbb{E}_{P_X}(S(x - X))$, where for $x \neq 0$, $S(x)$ denotes the projection on the unit sphere and $S(0) = 0$. Several other depth measures have been proposed for different kinds of data, for instance, *convex hull peeling depth* Barnett (1976), *Oja depth* Oja (1983), and *spherical depth* Elmore et al. (2006), among others. Some of them can be easily generalized to infinite-dimensional settings, like Tukey’s depth. However, this is not the case of some other ones, like Liu’s. In this setting, other notions of depths have been developed, see for instance Fraiman and Muniz (2001); López-Pintado and Romo (2009); Claeskens et al. (2014); Cuevas and Fraiman (2009). More recently, notions of depth have also been studied in general, non-Euclidean, metric spaces, see Fraiman et al. (2019). We refer to Serfling and Zuo (2000), which discuss properties that a depth measure should have (like, for instance, vanishing at infinity). However, some of these properties can not be extended to general metric spaces.

In this paper we will focus on the *lens depth* (denoted by LD), which was introduced in Liu and Modarres (2011), in \mathbb{R}^d ,

$$\text{LD}(x, P_X) = \mathbb{P}(x \in B(X_1, \|X_2 - X_1\|) \cap B(X_2, \|X_2 - X_1\|)), \quad x \in \mathbb{R}^d. \quad (1)$$

Here, $B(x, r)$ denotes the closed ball centred at x with radius r , and, as before, X_1, X_2 are independent random variables with common distribution P_X . It enjoys many good properties: for example, its computational complexity in \mathbb{R}^d is of order $O(n^2d)$, with n being the sample size (see Elmore et al. (2006)). This is considerably less than the empirical computational complexity of Tukey’s depth, $O(n^{(d-1)} \log(d))$, or Liu’s one, $O(n^{(d+1)})$.

Since this depth depends only on the distances between points (or any measure of similarity between them), it can be easily extended to any metric space (M, ρ) by replacing the norm in (1) with the distance ρ . In particular, this is the case when M is a Riemannian manifold and ρ is the geodesic distance. We will also prove, in this very general setting, that this depth has some of the desirable properties stated by Serfling. The empirical version of this depth for an iid sample X_1, \dots, X_n with distribution P_X is obtained by replacing P_X by the empirical distribution of the data, P_n . We show the consistency of the empirical version with the population one, and also provide the convergence rate. Another aim of our work is to introduce and study, for Riemannian manifolds, a more general version of this depth, which will be called the weighted lens depth. We will denote it by WLD_p . To build this depth measure, the idea is to take into account the underlying structure of the data, provided by the density of P_X , by changing the Riemannian metric on the manifold. For this generalized version we will also provide the convergence rate for the empirical version. It is important to note that for Riemannian manifolds embedded in \mathbb{R}^d , this empirical version can be computed and is consistent even if the Riemannian structure is unknown.

The classification problem for data on manifolds has recently gained importance, see for instance Yao and Zhang (2020) and the references therein. With a different approach, we will apply WLD_p on manifolds, to a classification method called the depth-depth, see Liu et al. (1999); Li et al. (2012); Cuesta-Albertos et al. (2017), and show the performance of the depth-depth method through the study of two real-life data sets.

Our construction enjoys three very nice properties. **Computational complexity:** Some depths (like Liu depth) are computationally infeasible in high dimensional problems, because their complexity grows exponentially with the dimension. This is not the case of lens depth. **Generality:** Lens depth (and also WLD_p) easily extends to general metric spaces and in particular to Riemannian manifolds. **Level-set structure:** Some depths (under restrictive conditions like unimodality or symmetry) characterize the distribution of the data, Kong and Zuo (2010); Kotík and Hlubinka (2017), and have convex level sets. However, if the aforementioned very restrictive conditions are not fulfilled, the level sets are not convex, see Dutta et al. (2011). Except for the case of distributions with convex support (see Hlubinka and Vencalek (2013)), the classical notions of depth are not designed to capture the underlying structure of the distribution. For instance, the balls defining the lens depth are balls with respect to the norm, and they do not take into account the density of the data. This makes the aforementioned classification method perform badly. To overcome this issue, several modifications of the classical notions of depths have been proposed. For instance in Kotík and Hlubinka (2017) a weighted Tukey’s depth is considered.

As shown in Li et al. (2012), the depth-depth approach behaves better than other learning procedures when the data have some non-standard patterns.

The first example of the application of the aforementioned depth-depth technique (see Cuesta-Albertos et al. (2017)) will be a classification problem where we have two classes, both of sample size 100. The data points are shown in Figure 1. We choose at random 50 of the 200 original sample points to use as a test sample. We apply Random Forest, trained with the pairs $(\widehat{\text{TD}}_0(X_i), \widehat{\text{TD}}_1(X_j))_{i,j}$, for $i, j = 1, \dots, 150$, where $\widehat{\text{TD}}_1(X_i)$ is Tukey’s depth of

X_i w.r.t. the 1-class, and $\widehat{\text{TD}}_2(X_i)$ is Tukey's depth of X_i w.r.t. the 2-class, see Figure 2. The misclassification error rate over 1000 replications was 10%. If we do the same but using WLD_p with $p = 2$, the misclassification error rate obtained was 1%.

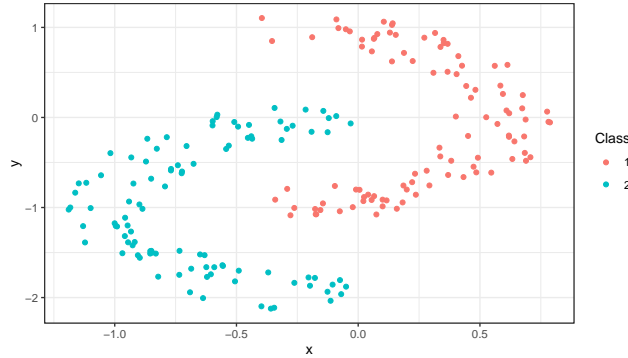


Figure 1: 200 data points for Example 1.

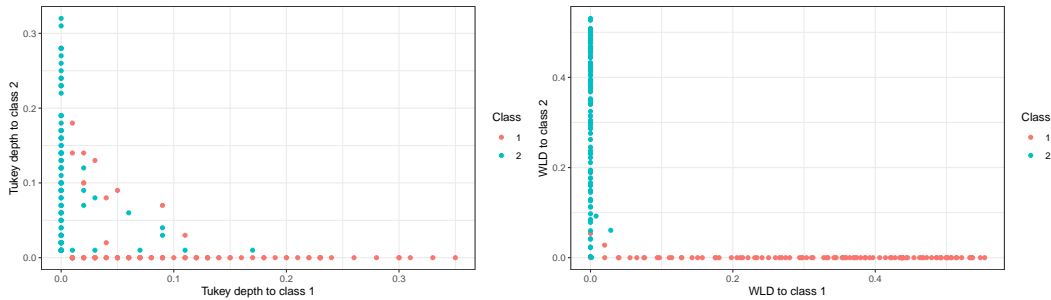


Figure 2: Depth-depth plots for the data shown in Figure 1. Left Panel: Results using Tukey's depth. Right Panel: Results using WLD_p with $p = 2$.

1.1 Outline

This paper is organized as follows. Section 3 extends the concept of lens depth to metric spaces and proves some of its properties. Section 4 introduces the concept of weighted lens depth and its estimator for data valued in a Riemannian manifolds. Consistency as well as convergence rates are obtained. Section 6 uses WLD_p in a supervised classification by means of the depth-depth method, for simulated data and for examples of real-life data. All proofs are postponed to the Appendix.

2 Notation

In what follows, (M, d) is a complete separable metric space, endowed with the Borel σ -algebra. The closed ball centred at x of radius $r > 0$ is denoted by $B(x, r)$. We denote by X (or more generally for $j \in \mathbb{N}^*$, X_j) an M -valued random variable, whose distribution is denoted by P_X . Given a set $A \subset M$, ∂A denotes its boundary. Given $\epsilon > 0$, we set $A^\epsilon = \{x \in M : d(x, A) \leq \epsilon\}$ (sometimes also denoted by $B(A, \epsilon)$). For $x \in M$, we write $d(x, A) = \inf_{a \in A} d(x, a)$. Given two non-empty compact sets A, C , their Hausdorff distance $d_H(A, C)$ is defined by

$$d_H(A, C) = \max \left\{ \max_{a \in A} d(a, C), \max_{c \in C} d(c, A) \right\}. \quad (2)$$

Given $x, y \in M$, we set $A(x, y) = B(x, d(x, y)) \cap B(y, d(x, y))$.

3 Lens depth on metric spaces

Recall that we have defined in (1), for $x \in M$, the lens depth of x to be $LD(x, P_X) = \mathbb{P}(X \in A(X_1, X_2))$. Given an iid sample $\mathcal{X}_n = \{X_1, \dots, X_n\} \subset M$ of a random variable X taking values in M , the empirical version of LD is defined by

$$\widehat{LD}_n(x) = \binom{n}{2}^{-1} \sum_{1 \leq i_1 < i_2 \leq n} \mathbb{1}_{A(X_{i_1}, X_{i_2})}(x). \quad (3)$$

Let us observe that $\widehat{LD}_n(x)$ is a U-statistic of order 2. In the next section, we extend, to general metric spaces, some properties of LD and $\widehat{LD}_n(x)$ which hold in the finite dimensional setting.

3.1 Some properties

In this section we will recall some desirable properties of the depth LD (see Serfling and Zuo (2000) or Fraiman et al. (2019)), for metric spaces. To prove the continuity of LD, we will make an assumption on the random variable X . Namely, we assume

$$\mathbb{P}(d(X, x_1) = d(X, x_2)) = 0, \quad \text{for all } x_1, x_2 \in M, x_1 \neq x_2. \quad (4)$$

In n -dimensional Euclidean space, this condition is equivalent to assuming that the $(n-1)$ -dimensional linear subspaces have probability zero. If condition 4 holds, then given $x \in M$,

$$\mathbb{P}(d(X_1, x) = d(X_1, X_2)) = \int_M \mathbb{P}(d(X_1, x) = d(X_1, t)) dP_X(t) = 0. \quad (5)$$

Proposition 1. (*Vanishing at infinity*). *Let (M, d) be a separable and complete metric space such that there exists z_0 with $\sup_{t \in M} d(z_0, t) = \infty$. Let $y \in M$ be fixed. Then,*

(a) $\sup_{d(x,y) > K} LD(x) \rightarrow 0$ as $K \rightarrow +\infty$, and

(b) $\lim_{K \rightarrow \infty} \sup_{d(x,y) > K} \widehat{LD}_n(x) = 0$ a.s.

Proposition 2. (*Continuity and point-wise consistency*). *Let $x, y \in M$ and assume that X satisfies (4). Then,*

(a) (*Continuity*) $|LD(x) - LD(y)| \rightarrow 0$ when $d(x, y) \rightarrow 0$.

(b) (*Consistency-rate of convergence*) $\beta_n |\widehat{LD}_n(x) - LD(x)| \rightarrow 0$ a.s. for all $\beta_n \rightarrow \infty$ such that $n/(\beta_n^2 \log(n)) \rightarrow \infty$.

4 Weighted lens depth on manifolds

4.1 Basic concepts

We will start by introducing briefly some basic concepts of Riemannian geometry, that will be used throughout this section. A Riemannian manifold is defined by a differentiable manifold M of dimension d , equipped with a Riemannian metric g_1 which defines for every point $p \in M$ the scalar product of tangent vectors in the tangent space $T_p M$, smoothly depending on the point p .

Given two points $x, y \in M$ the *induced distance* between them is defined as the infimum of the lengths $L(\gamma)$ of all continuously differentiable curves $\{\gamma_t\}_{t \in [0,1]} \subset M$ joining x and y .

A geodesic (with speed $s \in \mathbb{R}_0^+$) is a smooth map $\alpha : I \rightarrow M$, where I is an interval, such that $\|\alpha'(t)\| = s$ for all $t \in I$ and which is ‘‘locally length minimizing’’.

Through this section we assume that (M, g_1) is a d -dimensional Riemannian manifold without boundary (which is assumed to be unknown), and the available data is an iid sample $\mathcal{X}_n = \{X_1, \dots, X_n\} \subset M$ of a random vector X whose distribution P_X is assumed to be supported on M . We assume it has a density f w.r.t. the volume form on M given by the metric g_1 , see Petersen (2006). In this setting, to compute the empirical lens depth (defined by (3)) requires computing the geodesic distance between two points. This is a problem that has been previously tackled in the literature (see for instance Cormen et al. (2009) and Davis et al. (2019)). We will introduce a more general version of the lens depth, which will be called the weighted lens depth, that takes into account the density f together with the underlying Riemannian structure.

Given a parameter $p \geq 1$ (called the power parameter), we define a new metric $g_p = f^{2(p-1)/d} g_1$, see Hwang et al. (2016). The geodesic distance w.r.t. g_p between $x, y \in M$, is denoted by $\rho_p(x, y)$. Let $A \subset M$ be a locally finite set, that is $A \cap B$ is a finite set for any $B \subset M$ of finite volume w.r.t. g_1 . We define $L_p(x, y; A)$ by

$$L_p(x, y; A) = \min_{\{x_0=x, \dots, x_k=y\} \subset A^*} \sum_{i=0}^{k-1} (\rho_1(x_i, x_{i+1}))^p,$$

where $A^* = A \cup \{x, y\}$. We denote by $B_p(x, r)$ the closed ball of radius r , w.r.t. ρ_p , centred at x . We have

$$\rho_p(x, y) = \inf_{\gamma} \int_0^1 f(\gamma_t)^{(1-p)/d} \sqrt{g_1(\gamma'_t, \gamma'_t)} dt, \quad (6)$$

where $\{\gamma_t\}_{t \in [0,1]} \subset M$ is a piece-wise C^∞ -curve such that $\gamma_0 = x$ and $\gamma_1 = y$. The distance define by (6) is called Fermat distance. As mentioned in Groisman et al. (2018), "it coincides with Fermat principle in optics for the path followed by light in a non-homogeneous media when the refractive index is given by $f^{-\beta}$ ".

In Hwang et al. (2016) the following result is proven. It gives the (asymptotic) relation between ρ_p and $L_p(x, y; \mathcal{X}_n)$.

Theorem 1. (*Hwang–Damelin–Hero, 2016*) *Assume that the density f of X is continuous and bounded from below by a positive constant. Then, there exists a constant $C(d, p) > 0$ such that for all $\epsilon > 0$ and $b > 0$, there exists a $\theta_0 > 0$ such that, for n large enough.*

$$\mathbb{P}\left(\sup_{x, y \in M, \rho_1(x, y) \geq b} \left| \frac{L_p(x, y; \mathcal{X}_n)}{n^{(1-p)/d} \rho_p(x, y)} - C(d, p) \right| > \epsilon\right) \leq \exp(-\theta_0 n^{1/(d+2p)}),$$

If $p = 1$, it can be proved that $C(d, p) = 1$ (see Hwang et al. (2016)). It is important to note that neither θ_0 nor $C(d, p)$ depend on n . A similar version of the previous theorem is stated in McKenzie and Damelin (2019), with weaker assumptions, (the geodesic distance ρ_1 is replaced by the Euclidean norm $\|x_{i+1} - x_i\|$). They also address the clustering problem on manifolds. If the manifold is unknown, then ρ_1 in the definition of $L_p(x, y; A)$ can be replaced by the Euclidean distance, as in Groisman et al. (2018) or in McKenzie and Damelin (2019). We extend our previous notations by defining the set $A_p(x_1, x_2) = B_p(x_1, \rho_p(x_1, x_2)) \cap B_p(x_2, \rho_p(x_1, x_2))$ whose empirical version is $A_{p,n}(x_1, x_2) = A_{p,n}^1(x_1, x_2) \cap A_{p,n}^2(x_1, x_2)$, where $A_{p,n}^i(x_1, x_2) = \{t \in M : L_p(t, x_i, \mathcal{X}_n) < L_p(x_1, x_2, \mathcal{X}_n)\}$ $i = 1, 2$. As will be shown in the following example, these sets depend heavily on the choice of p .

Example 1. *To see how the shape of the level sets of WLD_p varies with p , let us consider the density $f(u, Ku) = C \exp\{-((u - u_0)\alpha^{-1})^2 - ((Ku - Ku_0)\beta^{-1})^2\}$, with $u, Ku \geq 0$,*

where $u_0 = 0.2$, $\beta = 0.5$, $Ku_0 = 30$, $\alpha = 3$ and C is the normalization constant. In Figure 3, the densities of the orthogonal and parallel components are shown, i.e. $x = uKu$ and $y = \sqrt{u^2 - x^2}$, based on a sample of size 200. This density has important applications when modelling electron-cyclotron-maser (ECM) instability and models for electron energization, see Tong et al. (2017). As can be seen in Figure 3, the sets $A_{2,200}^i(x_1, x_2)$ adapt their geometry to the level sets of the density. This effect does not appear in $A_{1,200}^i(x_1, x_2)$, since for $p = 1$ this set depends only on the extremes x_1, x_2 .

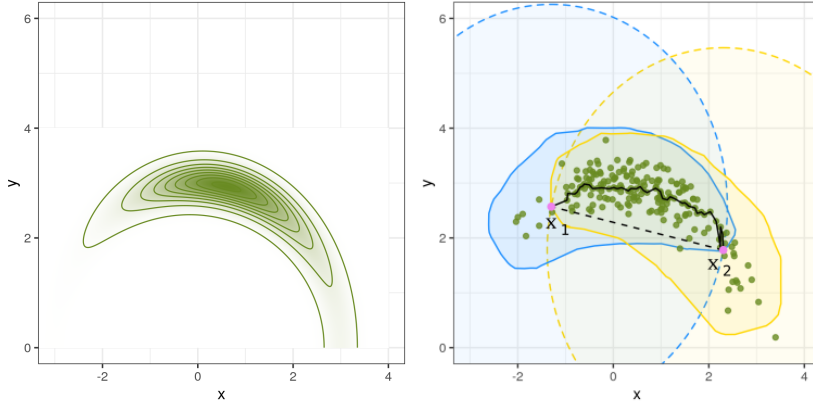


Figure 3: Left panel: Level sets of the density. Right panel: The sets $A_{1,n}^1(x_1, x_2)$ and $A_{1,n}^2(x_1, x_2)$ in blue, while $A_{2,n}^1(x_1, x_2)$ and $A_{2,n}^2(x_1, x_2)$ are shown in yellow. Sample points are shown in green. The black dotted line shows the geodesic joining x_1 and x_2 for $p = 1$. The piece-wise black curve is the geodesic joining x_1 and x_2 for $p = 2$.

4.2 Main results

With the previous notations we define the weighted lens depth of a point $x \in M$, of order p , denoted by $\text{WLD}_p(x)$, by

$$\text{WLD}_p(x) = \mathbb{P}(x \in A_p(X_1, X_2)) = \int_{M^2} \mathbb{1}_{A_p(x_1, x_2)}(x) P_X(dx_1) P_X(dx_2).$$

The empirical version of WLD_p , is given by the following U -statistic of order two:

$$\widehat{\text{WLD}}_{p,n}(x) := \binom{n}{2}^{-1} \sum_{1 \leq i_1 < i_2 \leq n} \mathbb{1}_{A_{p,n}(X_{i_1}, X_{i_2})}(x).$$

4.3 Consistency of the estimator

In order to prove that $\widehat{\text{WLD}}_{p,n}(x)$ is a consistent estimator, we first prove a lemma about the Hausdorff distance between the sets $B_p(x_1, \rho_p(x_1, x_2))$ and its empirical counterpart $A_{p,n}^1(x_1, x_2)$, where the Hausdorff distance d_H is computed using (2) for $d = \rho_1$.

Lemma 1. *Under the assumptions of Theorem 1, let $x_1, x_2 \in M$ and $\delta > 0$, there exists $\theta_0 > 0$ such that, for $i = 1, 2$, $\mathbb{P}(d_H(B_p(x_i, \rho_p(x_1, x_2))), A_{p,n}^i(x_1, x_2)) > \delta) \leq \exp(-\theta_0 n^{1/(d+2p)})$, for n large enough, where θ_0 is the constant given in Theorem 1.*

As a direct consequence of this lemma, we have the following corollary.

Corollary 1.

1) For $i = 1, 2$, $d_H(B_p(x_i, \rho_p(x_1, x_2)), A_{p,n}^i(x_1, x_2)) \rightarrow 0$ a.s., as $n \rightarrow \infty$.

2) For n large enough, $P(d_H(A_p(x_1, x_2), A_{p,n}(x_1, x_2)) > \delta) \leq 2 \exp(-\theta_0 n^{1/(d+2p)})$.

Condition I. We will say that a manifold (M, g_1) fulfils condition I if for all $p \in M$, $\partial B_1(p, \gamma)$ has positive reach for almost all $\gamma \in \mathbb{R}^+$ w.r.t. the Lebesgue measure on \mathbb{R} .

Recall that the reach of a set $A \subset (M, d)$ is defined as $\sup_{r \in \mathbb{R}} \{\forall x \in M, \text{ for which } d(x, A) < r, \text{ there exists a unique point } y \in A \text{ such that } d(x, y) = d(x, A)\}$.

Theorem 5.3 in Rataj and Zajíček (2009) states that condition I is fulfilled in dimensions 2 and 3 if the manifold M is complete.

Theorem 2. Under the hypotheses of Theorem 1. Assume that M fulfils condition I. Assume further that the density f is C^2 .

Then, for all $x \in M$,

$$\beta_n |\widehat{WLD}_{p,n}(x) - WLD_p(x)| \rightarrow 0 \text{ a.s., as } n \rightarrow \infty, \text{ where } n/(\beta_n^2 \log(n)) \rightarrow \infty. \quad (7)$$

5 Level sets of WLD_p in \mathbb{R}^2

We start by considering two distributions on the plane: a bivariate exponential distribution and an uniform distribution on a ring. We will study the shapes of the level sets when varying $p \in \{1, 1.5, 2, 5\}$, for a sample of size $n = 400$. Let us recall that for $p = 1$, we obtain the usual lens depth with the Euclidean distance. Two main scenarios are considered. (a) Bivariate exponential, with density $f(x, y) = e^{-x-y}$ with $x, y > 0$. (b) Uniform distribution on the ring $B((0, 0), 1.5) \setminus B((0, 0), 1)$.

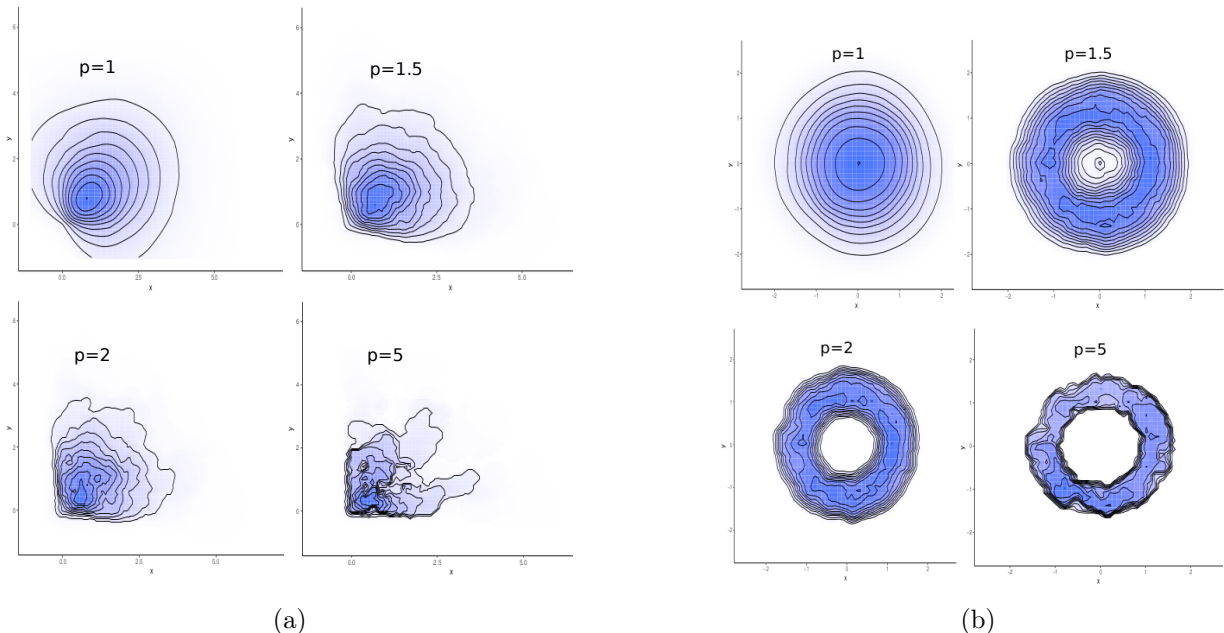


Figure 4: (a) Level sets of a sample of 400 exponentially distributed data-points. (b) Level sets of a sample of 400 uniformly distributed data-points on a ring.

Figures 4a and 4b show how with increasing p the level sets of WLD adapt to the support of the distribution, even for non-convex level sets. This is not the case with classical depths such as Tukey's or Liu's one.

6 Classification with depth-depth-G and WLD_p

The idea to use a depth measure as dimension reduction tool to perform classification was considered in Liu (1990). The method is called the depth-depth method, and is based on the depth-depth plots. This method was improved in Li et al. (2012) and Cuesta-Albertos et al. (2017). In these proposals, after a reduction to dimension two (implementing the depth-depth method), a classifier is applied. We will refer to this method as depth-depth-G.

To explain the procedure, let us assume that we have two classes and a depth D . Then the depth-depth method assigns to each point x a two dimensional vector, whose coordinates are its depth in each group. That is, $x \rightarrow (D_1(x), D_2(x))$, where, for $i = 1, 2$, $D_i(x)$ is the depth of x in the class i . Finally, a classification method (for instance SVM, Random Forest, k -NN, neural networks) is applied, in dimension two. This procedure can be easily generalized to several classes, or to product spaces, considering a depth on each component. Moreover, more than one depth can be used for each space.

This method is a dimensionality reduction procedure and also a new and useful visualization technique, see Ali et al. (2016).

6.1 Simulations

Example 1: Interlocking rings (in \mathbb{R}^2)

In this example, we show how the value of p captures different patterns that contribute to the classification. We consider as an example the ‘interlocking rings’ model. Let \mathbf{X} be a two-dimensional random vector, defined by $\mathbf{X} = ((2 + R) \cos \theta, (2 + R) \sin \theta)$, where R and θ are independent random variables, with $R \sim \text{Exp}(1/2)$ and $\theta \sim \text{Unif}(0, 2\pi)$. We generated 300 independent copies with distribution $\mathbf{X}_1 = \mathbf{X}'_1 + (3, 0)$ (group 1) and 300 from \mathbf{X}_2 (group 2), where \mathbf{X}'_1 and \mathbf{X}_2 are independent copies of \mathbf{X} , (see Figure 5). We considered 70% of the data for the training sample, and 30% for validation.

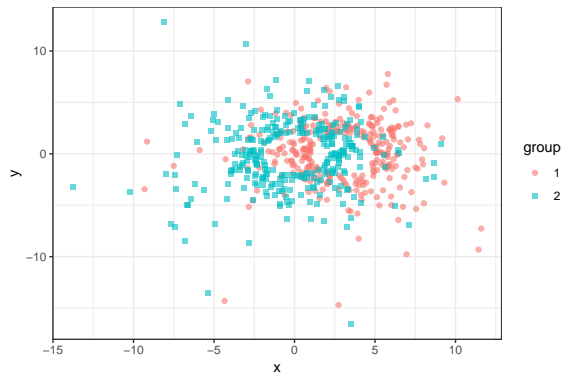


Figure 5: Sample points from the ‘interlocking rings’ model

We compared the performance of 1) Random Forest (RF), with the original sample; 2) depth-depth method with lens depth, and as the second step, RF in dimension 2; 3) depth-depth-G with WLD_p and $p = 1$ and 10, and as the second step, RF in dimension four; 4) depth-depth-G with WLD_p and $p = 1, 1.5, 2, 3, 5, 10$, and as the second step, RF in dimension 12. Figure 6 shows the depth-depth plots for $p = 1$ and $p = 10$.

The misclassification errors are shown in Table 1. The main conclusion is that, depth-depth-G with WLD_p and $p = 1, 1.5, 2, 3, 5, 10$ outperforms the other competitors.

Let us consider case 4), whose classification error is the smallest. We studied the importance of the variables in the classification, using *Mean Decrease Accuracy*, (see Breiman (2001)).

Table 1: Misclassification errors

1) RF	depth-depth with WLD_p and RF		
	2) $p = 1$	3) $p = 1, 10$	4) $p = 1, 1.5, 2, 3, 5, 10$
0.28	0.26	0.22	0.19

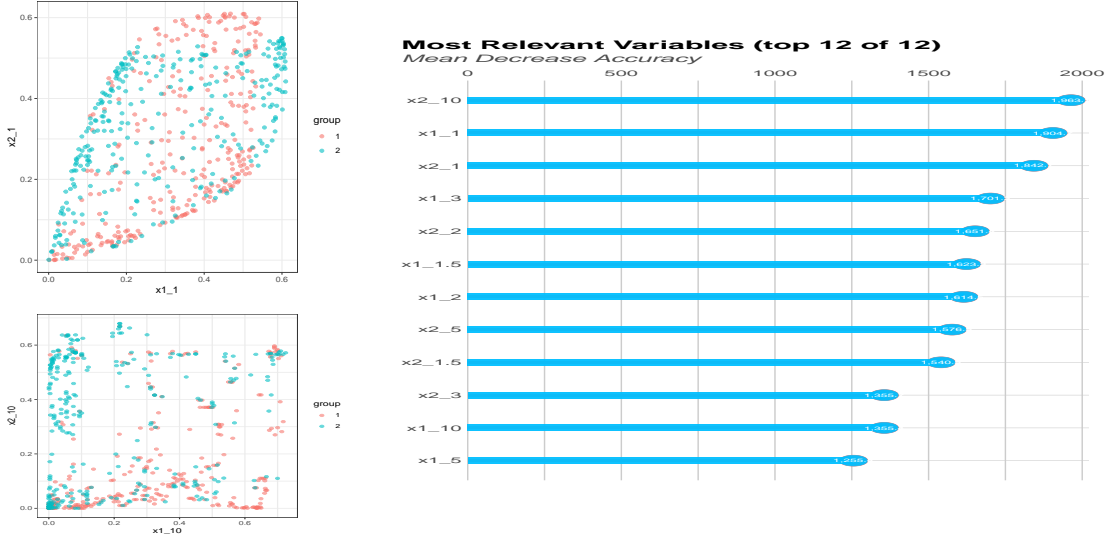


Figure 6: Top left Panel: Depth-depth plot for WLD_1 . Bottom left panel: Depth-depth plot for WLD_{10} . Right panel: Variable importance for RF.

Indeed, they depend on the parameter p , see Figure 6. This also suggests that taking differing values of p in WLD_p leads to differing contributions to the classification.

Example 2: The cone of positive definite matrices

Consider \mathcal{C}_k , the set of all $k \times k$ positive definite matrices. We will compare depth-depth-G using WLD_p with RF, on a binary classification problem on \mathcal{C}_k . Given two matrices $A, B \in \mathcal{C}_k$, the geodesic distance is given by $d(A, B) = \|\ln(A^{-1/2}BA^{-1/2})\|$, where $\|\cdot\|$ is the Hilbert–Schmidt norm (i.e., $\|A\| = \text{trace}(AA^t)$ being A^t the transpose of A), see Moakher (2005). Also, there exists a unique geodesic joining A and B (see Moakher (2005)), given by $\gamma(s) := A^{1/2}(A^{-1/2}BA^{-1/2})^s A^{1/2}$. To generate matrices with the Wishart distribution, we first choose a covariance matrix Σ and a positive integer m . Second, we generate a sample of m iid random variables with common distribution $N(0, \sigma)$. Then the matrix $S := \sum_{i=1}^m X_i X_i^\top$ has a Wishart distribution, i.e. $S \sim \mathcal{W}(\Sigma, m)$ on \mathcal{C}_5 .

In \mathcal{C}_5 , we will consider two iid samples of size n , following different Wishart distributions, each of them corresponding to a different group. For the first group we choose $m_1 = 10$ and $\Sigma_1 = I_5$. For the second group we choose $m_2 = 10$ and $\Sigma_2 = 2I_5$. The sample sizes in our study are $n = 100, 200, 300$. From each sample we choose 25% for validation. For the depth-depth method, we used first the lens depth, and as the second step RF. Figure 7 we display the depth-depth plot for $n = 300$, with WLD_2 , and RF. The misclassification error in that figure is 7%. We performed a simulation study to compare depth-depth-G and WLD_p with RF for $p = 1, 1.5, 2, 5$, k -nearest neighbour (k -NN) classifier for $k = \lceil n/10 \rceil$. The results are displayed in Table 2. The whole procedure was replicated 100 times. The conclusion is that depth-depth-G and WLD_p with RF outperforms k -NN in all cases, and the best value for the parameter p is $p = 2$.

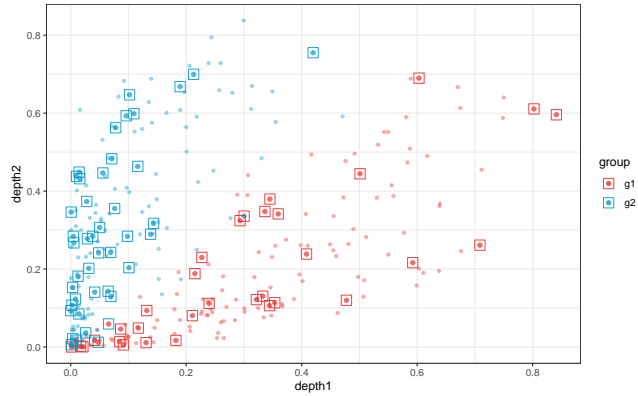


Figure 7: The result of the classification based on depth-depth-G with WLD_2 and RF, for $n = 300$. The colour of the circle shows the group to which each sample belongs. The square shows the validation sample. The colour of the square correspond to the group assigned.

Sample size	depth-depth-G and WLD_p , with RF				k -n.n
	$p = 1$	$p = 1.5$	$p = 2$	$p = 5$	
$n=100$	0.20	0.14	0.11	0.18	0.24
$n=200$	0.12	0.08	0.09	0.16	0.20
$n=300$	0.10	0.08	0.09	0.18	0.21

Table 2: Misclassification error for the positive definite matrices

6.2 An analysis of some real-life data

6.2.1 The manifold of phylogenetic trees

In this section, we focus on two examples arising from genetics. In both examples, the information contained in a genetic chain is approximated, represented, and analysed by means of a sample of low-complexity phylogenetic trees. These trees are used in general to represent ancestral histories. For details on how to build these trees and how to endow them with a Riemannian metric we refer to Billera et al. (2001). This manifold is complete and separable. An example of two of these trees is shown in Figure 8.

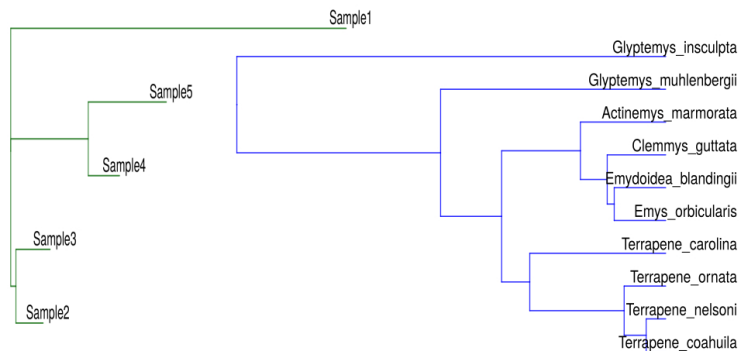


Figure 8: Left tree: A sample from the year 2001. Right tree: A sample from the gen ODC.

Example 3: Temporal analysis of influenza

As the first example, we use depth-depth-G on the manifold of phylogenetic trees, to analyse the evolution over time of the influenza virus. Modelling the genomic evolution of these viruses is an important issue (see Smith et al. (2004)). They mutate and evolve constantly,

becoming resilient to different drugs. Some examples are the Avian flu, SARS, and H2N2, among others. To be able to predict new genetic patterns is crucial to developing vaccines. Several statistical methodologies have been presented in the literature to understand this phenomenon, for example, in Solovyov et al. (2009), clusters of chains of genes are built to understand the pandemic of 2009.

We will focus on influenza of type A, H3N2, in particular, the subtype hemagglutinin (HA), since this subtype presents the largest variability in its genomic evolution and a strong resistance to standard vaccines, see Altman (2006). The data used here can be found in the GI-SAID EpiFluTM database ¹, which consists of the genomic data of 1089 sequences from 1993 to 2017 collected in New York. A pre-processing of the data is required, details of which can be found in Zairis et al. (2016); Monod et al. (2018).

The data-base was obtained from the GitHub repository <https://github.com/antheamonod/FluPCA>. Figure 8 (left tree) shows a tree from the sample of 2001.

We will use as a dimensionality reduction tool the depth-depth method between consecutive years, using LD with the geodesic distance. This is different from the PCA used in Monod et al. (2018); Nye et al. (2017). It allows a better visualization of the evolution of the different genetic orders, and the new kinds of strains, see Figure 9.

We may observe a clear difference between the strains of the virus from one year to the other, until 2003. Moreover, it seems that in some years (like 1999 or 2001), two different strains coexist. From 2003, the strains became more similar from one year to the other. It worth mentioning that the pandemic in 2009 is not detected by the diagrams because it involved H1N1 and we are analysing H3N2.

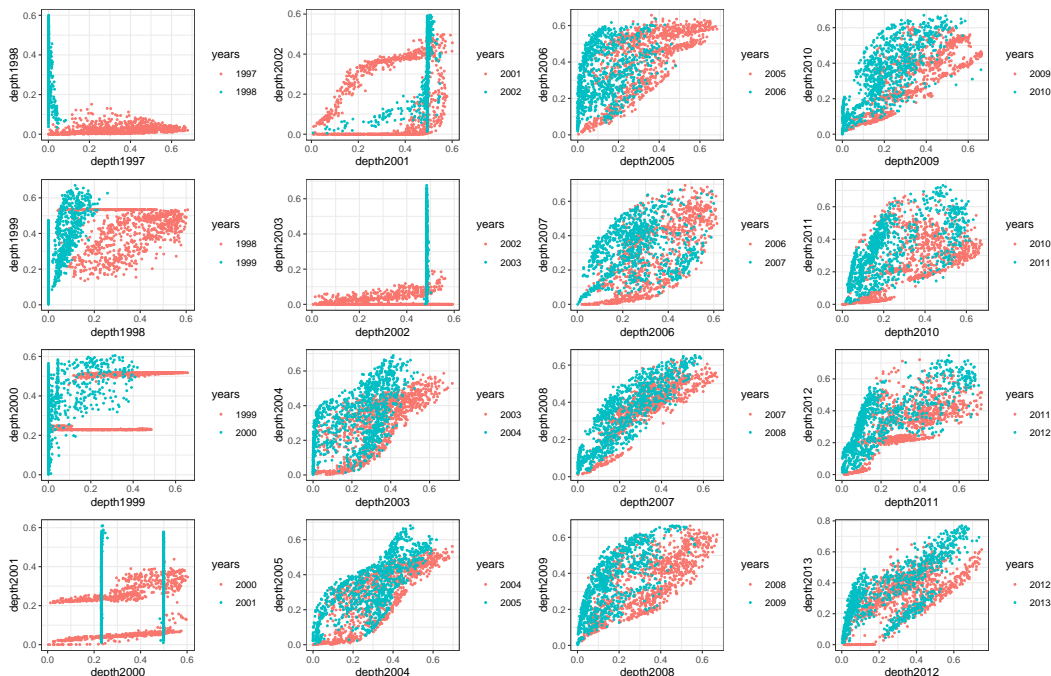


Figure 9: Depth-depth plots with lens depth for the sample of phylogenetic trees.

Example 4: Evolutionary trees for species of turtles

We will apply a similar approach to the evolutionary trees of the genes of species of turtles. The data-set consists of 1000 evolutionary trees. Each tree corresponds to one of ten possible

¹www.gisaid.org

genes (nine of them are of nuclear type, and the other is of mitochondrial type). There are 100 trees for each gene. The aim is to visualize the difference between the genes using lens depth. This problem is particularly difficult due to the large number of nodes on the evolutionary trees, (see Wiens et al. (2010)). A pre-processing of the data is performed (see Willis and Bell (2018) for details). Figure 8 (right) shows a tree of the species ODC. Using the depth-depth method with the lens depth on each gene, we have been able to find a clear difference between the mitochondrial type gene and the other nine nuclear genes. We have also been able to catch the differences between some nuclear genes, which the PCA used in Wiens et al. (2010) with two components was not able to capture. Figure 10 shows two different representations of the depths obtained (using LD): at the left, a circular diagram of the relative depths. Roughly speaking, the position of each point on the circle is based on the compositional-data depth of a tree on a given group, w.r.t. to its own group relative to the other nine groups (see Hoffman et al. (1999) for details of how these diagrams are built). On the right we show the parallel coordinate plot (we used the function `ggparcoord` of the R package `ggally`), that represents the absolute depths of the trees. Notice that the mitochondrial gene `cytb-codon` can be clearly differentiated from the other, nuclear, genes. Some genes present very different depths when compared to the others, for instance the genes `vim`, `Gapd` and `ODC`. However, some of them (such as `TGF`) present very high depths on their own gene, but also on the other genes, as can be seen in the parallel coordinate plot. This made the visualization problem much more involved.

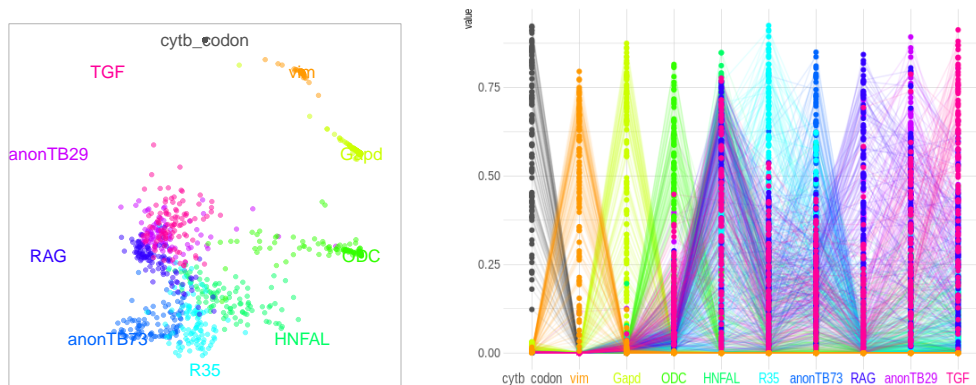


Figure 10: Depth for the sample of phylogenetic trees for species of turtles. Left panel: Weighted circular depth diagram for relative depths. Right panel: Parallel coordinate plot.

6.2.2 A signal recognition problem

A widely studied problem in signal recognition is how to automatically identify the nationality of a person when the available data is a sample of recorded words pronounced by a group of people, (see for instance Dhanalakshmi et al. (2009)). We used a data-base consisting of 329 people, from 6 different nationalities, where each of them pronounces a word in English.

The data-base can be downloaded from <https://archive.ics.uci.edu/> (see Fokoue (2020)). Each signal was preprocessed using the MFCC (Mel-Frequency Cepstral Coefficients) method, see Pedersen and Diederich (2008) and Ma and Fokoué (2014). The countries considered were Spain, France, Germany, the USA, Italy and England, with sample sizes 29, 30, 30, 165, 30 and 45, respectively. There is a reasonable balance with respect to the gender of the participants. As can be seen in Figure 11, a good performance is obtained by the depth-depth method with WLD_5 . For instance, there seems to be a clear separation between the Spanish and other nationalities, such as German or North American. In other cases, the pronunciation

is quite similar, for instance between Germans and North Americans. One can guess that this is due to the common evolutionary root of both languages.

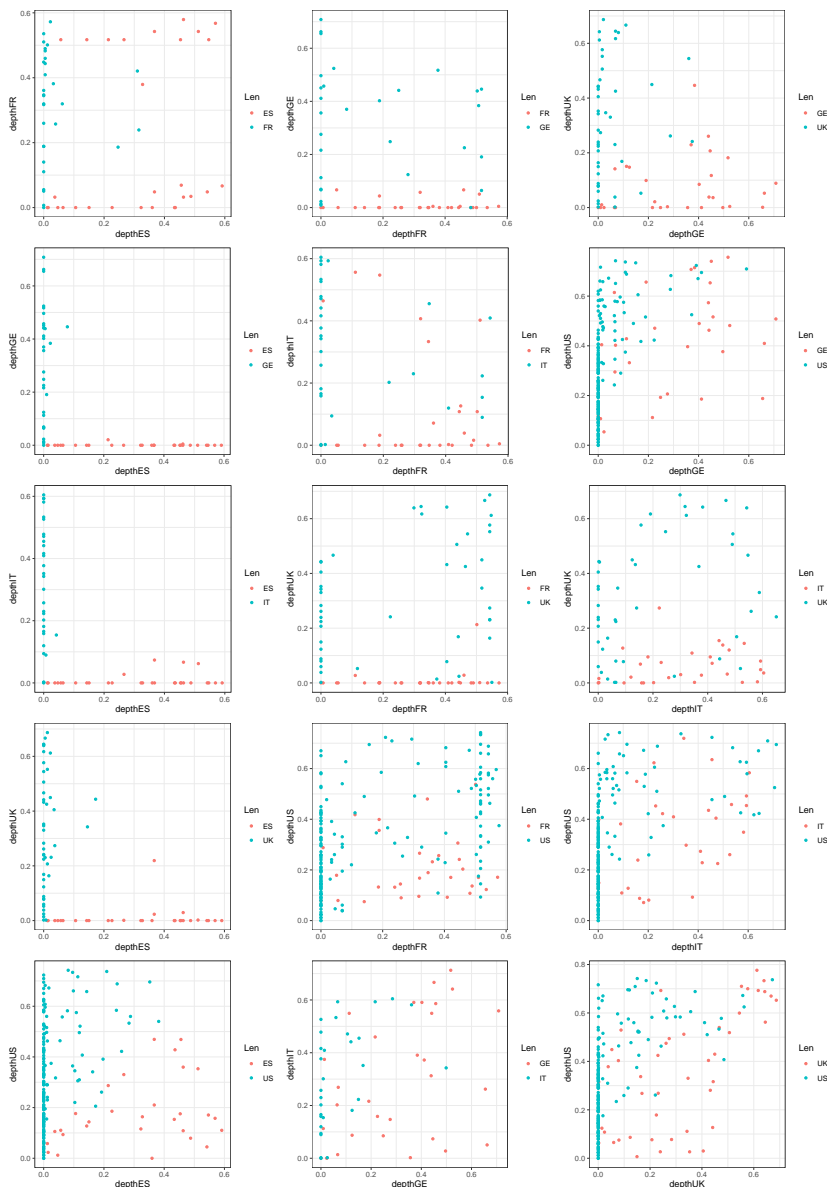


Figure 11: Depth-depth plots for WLD_5 , for all pairs of nationalities considered.

7 Concluding remarks

Studying depths on general metric spaces allows tackling problems where the structure of the data is neither finite dimensional nor functional. Some important examples, among others, are the phylogenetic trees given by the evolution of the history of genes, or data belonging to an unknown manifold. For separable and complete metric spaces, we have studied the main properties of the lens depth (LD), proved the consistency of the empirical version with the population one, and have provided almost parametric convergence rates. For Riemannian manifolds, we have provided an extension of LD, called WLD_p , which is more flexible than LD, and is able to also catch information about the geometry of the underlying distribution. We have also proved consistency results for the plug-in estimator of WLD_p . For most of the aforementioned problems, we showed, by using WLD_p , that it is crucial that the depth take into account not only the geometric structure of the data but also the underlying distribution. We use LD and WLD_p in supervised classification problem, putting in action the depth-depth

method introduced in Liu (1990). These classifications are performed on simulated and real life data examples. We obtain better performance than some competitors and interesting results on the real life data examples.

Appendix

Proof of Proposition 1

- (a) Let $x_1, x_2 \in M$, and write $R = d(x_1, x_2)$. Choose K large enough to ensure $x_1, x_2 \in B(y, K/3)$. If $d(x, y) > K$, it follows that $d(x_1, x) > 2K/3$. Then $x \notin B(x_1, R) \cap B(x_2, R)$. If X_1 and X_2 are independent copies of X , then $\text{LD}(x) = \mathbb{P}(x \in B(X_1, R) \cap B(X_2, R)) \leq 2\mathbb{P}(X \notin B(y, K/3))$ and $\mathbb{P}(X \notin B(y, K/3)) \rightarrow 0$ as $K \rightarrow \infty$.
- (b) Let us assume that (b) does not hold. Then there exists $\Omega_1 \subset \Omega$ with $\mathbb{P}(\Omega_1) = \delta > 0$ such that for all $\omega \in \Omega_1$ there exists $\gamma = \gamma(\omega) > 0$, and a sequence $K_n \rightarrow \infty$ such that $\sup_{\{x: d(x, y) > K_n\}} \widehat{\text{LD}}_n(x) > \gamma > 0$. Then for all $\omega \in \Omega_1$ and for all K , there exists $x = x(K)$ such that $d(x, y) > K$ and $\widehat{\text{LD}}_n(x) > \gamma$. Let K_0 be large enough to ensure $\mathbb{P}(d(y, X) > K_0/4) < \delta/(2n)$. Since $\Omega_1 \subset \{\omega : \text{there exists } i \text{ such that } d(y, X_i(\omega)) > K_0/4\}$, it follows that $\delta \leq n\mathbb{P}(d(y, X) > K_0/4) < \delta/2$, which is a contradiction. \square

Proof of Proposition 2

- (a) $|\text{LD}(x) - \text{LD}(y)| = \int_{M^2} |\mathbb{I}_{A(z,t)}(x) - \mathbb{I}_{A(z,t)}(y)| P_X(dz) P_X(dt)$. By definition, $1 = |\mathbb{I}_{A(z,t)}(x) - \mathbb{I}_{A(z,t)}(y)|$ if, and only if, either both $x \in A(z, t)$ and $y \notin A(z, t)$, or $x \notin A(z, t)$ and $y \in A(z, t)$. Set $d(x, y) = \epsilon$. In the first case, $x \in [\partial B(z, d(z, t))]^\epsilon \cup [\partial B(t, d(z, t))]^\epsilon =: \mathcal{E}_{z,t}^\epsilon$ and in the second case $y \in \mathcal{E}_{z,t}^\epsilon$. Then

$$\int_{M^2} |\mathbb{I}_{A(z,t)}(x) - \mathbb{I}_{A(z,t)}(y)| P_X(dz) P_X(dt) \leq \int_{M^2} \mathbb{I}_{\mathcal{E}_{z,t}^\epsilon}(x) P_X(dz) P_X(dt).$$

For any z, t , and x , $\mathbb{I}_{\mathcal{E}_{z,t}^\epsilon}(x) \rightarrow \mathbb{I}_{\mathcal{E}_{z,t}^0}(x)$ as $\epsilon \rightarrow 0$, so by the dominated convergence theorem, the integral converges to $2\mathbb{P}(x \in \partial B(X_1, d(X_1, X_2)))$. Lastly, (5), implies that $\mathbb{P}(x \in \partial B(X_1, d(X_1, X_2))) = 0$.

- (b) The proof is a straightforward consequence of the fact that the kernel of the U-statistic of order two $\widehat{\text{LD}}_n(x)$ is bounded between 0 and 1, together with Hoeffding's inequality for U-statistics, (see Serfling (1980), p. 201). This implies that for all $\delta > 0$ and $n > 2$,

$$\mathbb{P}\left(\beta_n |\widehat{\text{LD}}_n(x) - \text{LD}(x)| > \delta\right) \leq 2 \exp\left(-\frac{n}{\beta_n^2} C \delta^2\right), \quad (8)$$

with $C > 0$. Therefore, we may conclude applying the Borel–Cantelli Lemma. \square

Proof of Lemma 1

Let us define, for $\epsilon > 0$, $\Omega_1 = \{\omega : \sup_{x_1, x_2 \in M, \rho_p(x_1, x_2) \geq b} \left| \frac{L(x_1, x_2; \mathcal{X}_n)}{n^{(1-p)/d} \rho_p(x_1, x_2)} - C(d, p) \right| > \epsilon\}$, and $B = \overline{B_1(x_1, b)^c}$. Given $\delta > 0$, let $0 < b < \min\{\delta/6, \rho_p(x_1, x_2)\}$. By the triangle inequality,

$$\begin{aligned} \mathbb{P}\left(d_H[B_p(x_1, \rho_p(x_1, x_2)), A_{p,n}^1(x_1, x_2)] > \delta\right) \\ \leq \mathbb{P}\left(d_H[B_p(x_1, \rho_p(x_1, x_2)), B_p(x_1, \rho_p(x_1, x_2)) \cap B] > \delta/3\right) \\ + \mathbb{P}\left(d_H[B_p(x_1, \rho_p(x_1, x_2)) \cap B, A_{p,n}^1(x_1, x_2) \cap B] > \delta/3\right) + \\ + \mathbb{P}\left(d_H[A_{p,n}^1(x_1, x_2) \cap B, A_{p,n}^1(x_1, x_2)] > \delta/3\right) = J_1 + J_2 + J_3. \end{aligned}$$

From $d_H [B_p(x_1, \rho_p(x_1, x_2)) \cap B, B_p(x_1, \rho_p(x_1, x_2))] \leq \text{diam}(B^c) < \delta/3$, it follows that $J_1 = 0$. In the same way, $J_3 = 0$. Now J_2 is bounded from above by

$$\mathbb{P}(d_H [B_p(x_1, \rho_p(x_1, x_2)) \cap B, A_{p,n}^1(x_1, x_2) \cap B] > \delta/3 | \Omega_1^c) + \mathbb{P}(\Omega_1) = I_1 + I_2.$$

By Theorem 1, $I_2 \leq \exp(-\theta_0 n^{1/(d+2p)})$. Let us bound I_1 . By Theorem 1, for all $\omega \notin \Omega_1$,

$$n^\alpha \rho_p(x_1, x_2)(C(d, p) - \epsilon) \leq L(x_1, x_2; \mathcal{X}_n) \leq n^\alpha \rho_p(x_1, x_2)(C(d, p) + \epsilon),$$

$$\text{and } n^\alpha \rho_p(t, x_1)(C(d, p) - \epsilon) \leq L(x_1, t; \mathcal{X}_n) \leq n^\alpha \rho_p(t, x_1)(C(d, p) + \epsilon),$$

where $\alpha = (1-p)/d$. Let us define $C_+^+ = (C(d, p) + \epsilon)/(C(d, p) - \epsilon)$ and $C_+^- = (C(d, p) - \epsilon)/(C(d, p) + \epsilon)$, then for all $t \in B$

$$C_+^- \frac{\rho_p(t, x_1)}{\rho_p(x_1, x_2)} \leq \frac{L(t, x_1; \mathcal{X}_n)}{L(x_1, x_2; \mathcal{X}_n)} \leq C_+^+ \frac{\rho_p(t, x_1)}{\rho_p(x_1, x_2)}. \quad (9)$$

If we define $D^+ := B_p(x_1, C_+^+ \rho_p(x_1, x_2))$ and $D^- := B_p(x_1, C_+^- \rho_p(x_1, x_2))$ then from (9), $D^- \cap B \subset A_{p,n}^1(x_1, x_2) \cap B \subset D^+ \cap B$. Since $C_+^- < 1$ and $C_+^+ > 1$, $D^- \cap B \subset B_p(x_1, \rho_p(x_1, x_2)) \cap B \subset D^+ \cap B$. Further, conditioned on $\omega \notin \Omega_1$, for n large enough,

$$d_H [B_p(x_1, \rho_p(x_1, x_2)) \cap B, A_{p,n}^1(x_1, x_2) \cap B] \leq d_H [D^- \cap B, D^+ \cap B].$$

Observe that $d_H [D^- \cap B, D^+ \cap B] \rightarrow 0$ as $\epsilon \rightarrow 0$. So that, for ϵ small enough and n large enough, $I_1 = 0$. \square

Proof of Theorem 2

Let $\delta > 0$. $\mathbb{P}(|\widehat{\text{WLD}}_{p,n}(x) - \text{WLD}_p(x)| > 2\delta/\beta_n)$ is bounded from above by

$$\begin{aligned} & \mathbb{P}\left(\left|\binom{n}{2}^{-1} \sum_{1 \leq i_1 < i_2 \leq n} \mathbb{1}_{A_{p,n}(X_{i_1}, X_{i_2})}(x) - \mathbb{1}_{A_p(X_{i_1}, X_{i_2})}(x)\right| > \delta/\beta_n\right) + \\ & \mathbb{P}\left(\left|\binom{n}{2}^{-1} \sum_{1 \leq i_1 < i_2 \leq n} \mathbb{1}_{A_p(X_{i_1}, X_{i_2})}(x) - E(\mathbb{1}_{A_p(X_1, X_2)}(x))\right| > \delta/\beta_n\right) = I + II. \end{aligned}$$

The term II is bounded from above by $\exp(-Cn/\beta_n^2)$, arguing similarly as was done to prove (8) (with g_p instead of g_1), $C > 0$ being a constant. By Chebyshev inequality, I is bounded from above by $(\beta_n/\delta)\mathbb{E}[\mathbb{1}_{A_{p,n}(X_1, X_2) \Delta A_p(X_1, X_2)}(x)] = (\beta_n/\delta)\mathbb{P}(x \in A_{p,n}(X_1, X_2) \Delta A_p(X_1, X_2))$.

$$\begin{aligned} \mathbb{P}(x \in A_{p,n}(X_1, X_2) \Delta A_p(X_1, X_2)) = \\ \int_{M^2} \mathbb{P}(x \in A_{p,n}(x_1, x_2) \Delta A_p(x_1, x_2)) P_X(dx_1) P_X(dx_2). \quad (10) \end{aligned}$$

Let us bound $\mathbb{P}(x \in A_{p,n}(x_1, x_2) \Delta A_p(x_1, x_2)) \leq \mathbb{P}(x \in B(\partial A_p(x_1, x_2), \gamma))$, where $\gamma = d_H(A_{p,n}(x_1, x_2), A_p(x_1, x_2))$. Set $d_H = d_H(A_{p,n}(x_1, x_2), A_p(x_1, x_2))$, Let P_{d_H} denotes its law on \mathbb{R}^+ . Then,

$$\begin{aligned} & \int_{M^2} \mathbb{P}(x \in A_{p,n}(x_1, x_2) \Delta A_p(x_1, x_2)) P_X(dx_1) P_X(dx_2) = \\ & \int_{M^2} \int_0^{+\infty} \mathbb{P}(x \in B_1(\partial A_p(x_1, x_2), \gamma)) P_{d_H}(d\gamma) P_X(dx_1) P_X(dx_2) = \\ & \int_0^{d_{p_1}(M)} \left(\int_{M^2} \mathbb{P}(x \in B_1(\partial A_p(x_1, x_2), \gamma)) P_X(dx_1) P_X(dx_2) \right) P_{d_H}(d\gamma), \end{aligned}$$

where $d_{\rho_1}(M) = \max_{x,y \in M} \rho_1(x,y)$. Let $\gamma \in [0, d_{\rho_1}(M)]$ be fixed,

$$\begin{aligned} \int_{M^2} \mathbb{P}(x \in B_1(\partial A_p(x_1, x_2), \gamma)) P_X(dx_1) P_X(dx_2) &= \\ P_X \otimes P_X \{(x_1, x_2) \in M^2 : x \in B_1(\partial A_p(x_1, x_2), \gamma)\} &= \\ \int_M P_X\{x_1 \in M : x \in B_1(\partial A_p(x_1, x_2), \gamma)\} P_X(dx_2). & \end{aligned}$$

Let $f_0 = \max_{x \in M} f(x)$, and ν be the volume measure on M inherited from g_1 , then, for fixed γ and x_2 , $P_X\{x_1 \in M : x \in B_1(\partial A_p(x_1, x_2), \gamma)\} = P_X[B_1(\partial B_p(x_1, \rho_p(x, x_2)), \gamma)] \leq f_0 \nu(B_1(\partial B_p(x_1, \rho_p(x, x_2)), \gamma))$. From the dominated convergence theorem it follows easily that for fixed γ and x , the function $x_2 \rightarrow \nu(B_1(\partial B_p(x_1, \rho_p(x, x_2)), \gamma))$ is a continuous function of x_2 . Its maximum is reached at some $x_2^0 = x_2^0(\gamma)$. Let us bound $\nu(B_1(\partial B_p(x_1, \rho_p(x, x_2^0)), \gamma))$. By condition I, $\partial B_p(x_1, \rho_p(x, x_2^0))$ has positive reach w.r.t. ρ_p . Then by the Corollary on page 57 in Bangert (1982), it has positive reach $R > 0$ w.r.t. ρ_1 . So that, there exists a positive constant τ such that $\nu(B_1(\partial B_p(x_1, \rho_p(x, x_2^0)), \gamma)) = \tau\gamma$ for all $\gamma \in [0, R]$. This result was initially proved in Federer (1959) for subsets of \mathbb{R}^d and generalized to manifolds in Kleinjohann (1981).

Then I is bounded from above by

$$\beta_n \delta^{-1} f_0 \tau \int_0^R \gamma P_{d_H}(d\gamma) + \beta_n \delta^{-1} f_0 \int_R^{d_{\rho_1}(M)} \nu(B_1(\partial B_p(x_1, \rho_p(x, x_2^0)), \gamma)) P_{d_H}(d\gamma) = J_1 + J_2.$$

To bound J_2 multiply and divide the integral by γ , and bound $1/\gamma \leq 1/R$. So that, J_2 is bounded from above by

$$\beta_n \delta^{-1} f_0 \nu(M) R^{-1} \int_R^{d_{\rho_1}(M)} \gamma P_{d_H}(d\gamma) \leq \beta_n \delta^{-1} f_0 \nu(M) R^{-1} \int_0^{d_{\rho_1}(M)} P(d_H > \gamma) d\gamma. \quad (11)$$

Now J_1 is bounded from above by

$$\beta_n \delta^{-1} f_0 \tau \int_0^{d_{\rho_1}(M)} \gamma P_{d_H}(d\gamma) = f_0 \beta_n 2L_0 \delta^{-1} \tau \int_0^{d_{\rho_1}(M)} P(d_H > \gamma) d\gamma. \quad (12)$$

Corollary 1 implies that (11) and (12) are bounded from above by $C\delta^{-1}\beta_n \exp(-\theta_0 n^{1/(d+2p)})$. We may conclude that (7) holds using $n^{1/(d+2p)}/(\log(\beta_n) \log(n)) \rightarrow \infty$ and the Borel–Cantelli Lemma. \square

References

- Ali, S. M., Gupta, N., Nayak, G. K., and Lenka, R. K. (2016). Big data visualization: Tools and challenges. In 2016 2nd International Conference on Contemporary Computing and Informatics (IC3I), pages 656–660. IEEE.
- Altman, L. K. (2006). This season’s flu virus is resistant to 2 standard drugs. New York Times.
- Bangert, V. (1982). Sets with positive reach. Archiv der Mathematik, 38(1):54–57.
- Barnett, V. (1976). The ordering of multivariate data. Journal of the Royal Statistical Society. Series A (General), 139(3):318–355.

- Billera, L. J., Holmes, S. P., and Vogtmann, K. (2001). Geometry of the space of phylogenetic trees. Advances in Applied Mathematics, 27(4):733–767.
- Breiman, L. (2001). Random forests. Machine learning, 45(1):5–32.
- Claeskens, G., Hubert, M., Slaets, L., and Vakili, K. (2014). Multivariate functional halfspace depth. Journal of the American Statistical Association, 109(505):411–423.
- Cormen, T. H., Leiserson, C. E., Rivest, R. L., and Stein, C. (2009). Introduction to algorithms. MIT press.
- Cuesta-Albertos, J. A., Febrero-Bande, M., and de la Fuente, M. O. (2017). The dd^g -classifier in the functional setting. Test, 26(1):119–142.
- Cuevas, A. and Fraiman, R. (2009). On depth measures and dual statistics. a methodology for dealing with general data. Journal of Multivariate Analysis, 100(4):753–766.
- Davis, E., Sethuraman, S., et al. (2019). Approximating geodesics via random points. The Annals of Applied Probability, 29(3):1446–1486.
- Dhanalakshmi, P., Palanivel, S., and Ramalingam, V. (2009). Classification of audio signals using svm and rbfn. Expert systems with applications, 36(3):6069–6075.
- Dutta, S., Ghosh, A. K., Chaudhuri, P., et al. (2011). Some intriguing properties of tukey’s half-space depth. Bernoulli, 17(4):1420–1434.
- Elmore, R. T., Hettmansperger, T. P., and Xuan, F. (2006). Spherical data depth and a multivariate median. DIMACS Series in Discrete Mathematics and Theoretical Computer Science, 72:87.
- Federer, H. (1959). Curvature measures. 93(3):418–491.
- Fokoue, E. (2020). Uci machine learning repository.
- Fraiman, R., Gamboa, F., and Moreno, L. (2019). Connecting pairwise geodesic spheres by depth: Dcops. Journal of Multivariate Analysis, 169:81–94.
- Fraiman, R. and Muniz, G. (2001). Trimmed means for functional data. Test, 10(2):419–440.
- Groisman, P., Jonckheere, M., and Sapienza, F. (2018). Nonhomogeneous euclidean first-passage percolation and distance learning. arXiv preprint arXiv:1810.09398.
- Hlubinka, D. and Vencalek, O. (2013). Depth-based classification for distributions with nonconvex support. Journal of Probability and Statistics, 2013.
- Hoffman, P., Grinstein, G., and Pinkney, D. (1999). Dimensional anchors: a graphic primitive for multidimensional multivariate information visualizations. In Proceedings of the 1999 workshop on new paradigms in information visualization and manipulation in conjunction with the eighth ACM international conference on Information and knowledge management, pages 9–16.
- Hwang, S. J., Damelin, S. B., Hero III, A. O., et al. (2016). Shortest path through random points. The Annals of Applied Probability, 26(5):2791–2823.
- Kleinjohann, N. (1981). Nächste punkte in der riemannschen geometrie. 176.

- Kong, L. and Zuo, Y. (2010). Smooth depth contours characterize the underlying distribution. Journal of Multivariate Analysis, 101(9):2222–2226.
- Kotík, L. and Hlubinka, D. (2017). A weighted localization of halfspace depth and its properties. Journal of Multivariate Analysis, 157:53–69.
- Li, J., Cuesta-Albertos, J. A., and Liu, R. Y. (2012). Dd-classifier: Nonparametric classification procedure based on dd-plot. Journal of the American Statistical Association, 107(498):737–753.
- Liu, R. Y. (1990). On a Notion of Data Depth Based on Random Simplices. The Annals of Statistics, 18(1):405–414.
- Liu, R. Y. (1992). Data depth and multivariate rank tests. L1-statistical analysis and related methods (Y. Dodge, ed.), pages 279–294.
- Liu, R. Y., Parelius, J. M., Singh, K., et al. (1999). Multivariate analysis by data depth: descriptive statistics, graphics and inference, (with discussion and a rejoinder by liu and singh). The annals of statistics, 27(3):783–858.
- Liu, R. Y. and Singh, K. (1992). Ordering directional data: Concepts of data depth on circles and spheres. Ann. Statist., 20(3):1468–1484.
- Liu, Z. and Modarres, R. (2011). Lens data depth and median. Journal of Nonparametric Statistics, 23(4):1063–1074.
- López-Pintado, S. and Romo, J. (2009). On the concept of depth for functional data. Journal of the American Statistical Association, 104(486):718–734.
- Ma, Z. and Fokoué, E. (2014). A comparison of classifiers in performing speaker accent recognition using mfccs. Open Journal of Statistics, (4):258–266.
- Mckenzie, D. and Damelin, S. (2019). Power weighted shortest paths for clustering euclidean data. Foundations of Data Science, 1(3):307.
- Moakher, M. (2005). A differential geometric approach to the geometric mean of symmetric positive-definite matrices. SIAM Journal on Matrix Analysis and Applications, 26(3):735–747.
- Monod, A., Lin, B., Yoshida, R., and Kang, Q. (2018). Tropical geometry of phylogenetic tree space: A statistical perspective. arXiv preprint arXiv:1805.12400.
- Nye, T. M., Tang, X., Weyenberg, G., and Yoshida, R. (2017). Principal component analysis and the locus of the fréchet mean in the space of phylogenetic trees. Biometrika, 104(4):901–922.
- Oja, H. (1983). Descriptive statistics for multivariate distributions. Statistics & Probability Letters, 1(6):327–332.
- Pedersen, C. and Diederich, J. (2008). Accent in speech samples: Support vector machines for classification and rule extraction. In Rule extraction from support vector machines, pages 205–226. Springer.
- Petersen, P. (2006). Riemannian geometry, volume 171. Springer.

- Rataj, J. and Zajicek, L. (2009). Critical values and level sets of distance functions in riemannian, alexandrov and minkowski space.
- Serfling, R. (1980). Approximation theorems of mathematical statistics. Wiley series in probability and mathematical statistics : Probability and mathematical statistics. Wiley, New York, NY [u.a.], [nachdr.] edition.
- Serfling, R. (2002). A depth function and a scale curve based on spatial quantiles. In Statistical Data Analysis Based on the L1-Norm and Related Methods, pages 25–38. Springer.
- Serfling, R. and Zuo, Y. (2000). General notions of statistical depth function. The Annals of Statistics, 28(2):461–482.
- Smith, D. J., Lapedes, A. S., de Jong, J. C., Bestebroer, T. M., Rimmelzwaan, G. F., Osterhaus, A. D., and Fouchier, R. A. (2004). Mapping the antigenic and genetic evolution of influenza virus. science, 305(5682):371–376.
- Solovyov, A., Palacios, G., Briese, T., Lipkin, W. I., and Rabadan, R. (2009). Cluster analysis of the origins of the new influenza a (h1n1) virus. Eurosurveillance, 14(21):19224.
- Tong, Z.-J., Wang, C.-B., Zhang, P.-J., and Liu, J. (2017). A parametric investigation on the cyclotron maser instability driven by ring-beam electrons with intrinsic alfvén waves. Physics of Plasmas, 24(5):052902.
- Tukey, J. W. (1975). Mathematics and the picturing of data. In Proceedings of the international congress of mathematicians, volume 2, pages 523–531.
- Vardi, Y. and Zhang, C.-H. (2000). The multivariate l1-median and associated data depth. Proceedings of the National Academy of Sciences, 97(4):1423–1426.
- Wiens, J. J., Kuczynski, C. A., and Stephens, P. R. (2010). Discordant mitochondrial and nuclear gene phylogenies in emydid turtles: implications for speciation and conservation. Biological Journal of the Linnean Society, 99(2):445–461.
- Willis, A. and Bell, R. (2018). Uncertainty in phylogenetic tree estimates. Journal of Computational and Graphical Statistics, 27(3):542–552.
- Yao, Z. and Zhang, Z. (2020). Principal boundary on riemannian manifolds. Journal of the American Statistical Association, 115(531):1435–1448.
- Zairis, S., Khiabani, H., Blumberg, A. J., and Rabadan, R. (2016). Genomic data analysis in tree spaces. arXiv preprint arXiv:1607.07503.